

# Sorption of Thorium Using Magnetic Graphene Oxide Polypyrrole Composite Synthesized from Water Hyacinth Roots

**Gado, Mohamed\*<sup>+</sup>**

*Nuclear Materials Authority, 530 P.O. Box Maadi, Cairo, EGYPT*

**ABSTRACT:** Polypyrrole magnetic graphene oxide (PPy/MGO) composites have been synthesized from a natural source (water hyacinth roots) using polymerization technique for Th(IV) ions pre-concentration from aqueous solutions. The effects of controlling factor have been studied using the batch technique. The obtained results show that the maximum Th(IV) adsorption capacity by PPy/MGO composite is 277.8 mg/g at pH 4, which is higher than traditional adsorbents. PPy/MGO composite also presents excellent regeneration/reuse property. The PPy/MGO was thoroughly characterized by a number of techniques namely, Fourier transforms infrared, Raman, as well as X-ray diffraction, thermogravimetric and Energy-Dispersive X-ray (EDX). Due to the high adsorption capacity of Th (IV), PPy/MGO composite can be used in nuclear fuel achievement and for Th(IV) environmental pollution cleanup.

**KEYWORDS:** Thorium; Polypyrrole; Graphene oxide; Composite; Adsorption.

## INTRODUCTION

Due to the high toxicity of radioactive metals, especially uranium and thorium, exposure to these pollutants has been considered a quickly growing problem for human health, the presence of radionuclides and toxic metals in wastes is a major environmental concern. Such wastes arise from technologies producing nuclear fuels, and from laboratories working with radioactive materials, hence, removal of these heavy metals from polluted waters and wastewaters is very necessary [1-3]. Different kinds of traditional methods such as ion exchange, membrane filtration, sorption/adsorption, and solidification, have been applied to remove uranium and thorium ions from the aqueous solutions. Among these techniques, the economic

sorption method has been widely used to remove uranium and thorium ions because it is easy to operate and can be applied in large scale for possible practical applications. The sorption of U(VI) on oxides and clay minerals have been studied extensively [4-6]. Today, there is a growing interest for potential applications of sorption technology in metal separations, hydrometallurgy, water and wastewater treatment, removal and recovery of metal ions [7-15]. Several materials have been used as an adsorbent as clay minerals [16], silica [17], zeolite [18] which suffer from either low adsorption capacities or efficiencies compared with Graphene that exhibits high efficiency toward U(VI) and Th(IV). Recent studies indicate that carbon materials such as activated carbons [19],

---

\* To whom correspondence should be addressed.

+ E-mail: parq28@yahoo.com

1021-9986/2018/3/145-160

16/\$/6.06

carbon nanotube [20], and graphene [21] exhibit excellent adsorption capacity towards U(VI) and Th(IV).

Graphene oxides (GO), a kind of one or several atomic layered graphites, possess special two-dimensional structures and excellent electrical, mechanical and thermal properties [22]. Large amounts of oxygen-containing functional groups such as hydroxyl ( $-OH$ ) and epoxy groups ( $-O-$ ) on the surfaces along with the carboxyl

( $-COOH$ ) groups at the edge sites of GOs are generated during the Hummers synthesis process [23].

Graphene shows promise as a future material in sensors, drug delivery, composite materials, hydrogen storage, catalysis and solar cells due to its electrical, mechanical, optical and thermal characteristics [24–25]. Graphene Oxide (GO) as a precursor offers the possibility of cost-effective, large-scale production of graphene-based materials. Owing to the presence of plenty of hydroxyl, epoxy, carboxyl and carbonyl groups, oxygen functionality modifications can establish as active sites for anchoring ions and complexes [26].

Graphene has strong mechanical, thermal, and electrical properties, with a theoretical value of specific surface area at  $2630 \text{ m}^2/\text{g}$  [27]. Several reviews have been reported on applications of GO and GNs in different areas such as physics, chemistry, biology, and materials science [28–31], however, few reviews on graphene-based materials as adsorbents for pollutant removal is available [32].

Recently, hybrid graphene-based composites were synthesized using different materials, such as metal nanoparticles, boron nitride, metal oxides-based nanostructures and multilayer graphene [33–36]. Among these nanocomposites, the impact in the association of graphene with Au metallic nanoparticles producing nanocomposites has been much of interest because of their potential applications in biosensing, energy devices, catalytic and environmental fields. Polymer-graphene nanocomposites are very promising because the combination of graphene and polymer substantially improves the properties of the nanocomposites [37]. For example, polymethyl methacrylate/graphene nanocomposite shows better flame-retardant property than bare polymethyl methacrylate [38], and polylactic acid/graphene composites prepared by masterbatch-based melt blending has improved thermal degradation and combustion properties as compared with the bare polymer [39].

This study aims to figure out the preparation and characterization of PPy/MGO for thorium ions removal from acidic liquors.

## EXPERIMENTAL SECTION

### *Chemicals and reagents*

$\text{Th}(\text{NO}_3)_4 \cdot 5\text{H}_2\text{O}$  was obtained from Merck Co. The stock solution of Th(IV) was prepared by dissolving appropriate amounts of  $\text{Th}(\text{NO}_3)_4 \cdot 5\text{H}_2\text{O}$  in a nitric acid solution for inhibition of the hydrolysis of Th(IV). All other chemicals were of analytical grade and used without further purification. All testing solutions were prepared with de-ionized water.

### *GO preparation from Water hyacinth roots*

GO nanosheets were synthesized from graphitic material obtained from Water Hyacinth Roots (WHR) according to the following: The roots, leaves, and stems of the water hyacinth collected from river Nile in Mitghamer, Mansoura, Egypt were separated from each other, the roots were washed with distilled water then with very dilute acidified water (3% HCl) and were soaked in 0.25 M EDTA at pH 10 overnight to remove any metal ions adsorbed on the plant parts and washed with distilled water for several times and dried in oven at  $110^\circ\text{C}$  for 48 h, after that dried plant (roots, stems, and leaves) were ground and stored in desiccators till used in adsorption experiments.

Ten grams of dried roots carbonized at  $400\text{--}500^\circ\text{C}$  in the presence of nitrogen for about 8–10 hours, have been ground by mortar into powder form (about 331 mesh size).

Five grams from the obtained charcoal material have been mixed with 2.5%  $\text{FeCl}_3 \cdot 6\text{H}_2\text{O}$  (to activate the charcoal as well as increase the surface area; pH adjusted at 2), was stirred at  $60^\circ\text{C}$  for 5 hours, then left for 2 days for gradual water evaporation at room temperature and finally dried at  $100^\circ\text{C}$  for 5 hours to achieve a black solid material. The obtained graphitized material was ground by mortar to obtain a powder that was used in the next step.

The prepared graphitized material has been used as raw materials to synthesize GO using a modified Hummers' method. For this purpose, 5g of graphitized material and 2.5g of  $\text{NaNO}_3$  were mixed with 108mL  $\text{H}_2\text{SO}_4$  and 12mL  $\text{H}_3\text{PO}_4$ , stirred in an ice bath for 10min. Next, 15g  $\text{KMnO}_4$  was slowly added so that the temperature of the mixture remained below  $5^\circ\text{C}$ . The suspension was then reacted for 2h in an ice bath and stirred for 60min

before being stirred in a 40°C water bath for 60 min. The temperature of the mixture was adjusted to a constant 98°C for 60min while water was added continuously. Deionized water was further added so that the volume of the suspension was 400 mL. 15 mL of H<sub>2</sub>O<sub>2</sub> was added after 5 min. The reaction product was centrifuged and washed with deionized water and 5% HCl solution repeatedly. Finally, the product was dried at 60°C.

#### Preparation of magnetic graphene oxide MGO

The magnetic graphene oxide has been prepared using the modified method of Massart [40], where about 100 mL from ferric solution (0.2 M) has been mixed with 100 mL from freshly prepared 0.1 M ferrous solution under stirring with ten gram from the produced porous carbon. After that, about 100 ml from ammonia solution (30 %) has been poured to the Fe<sup>3+</sup>/Fe<sup>2+</sup>/GO mixture and stirred vigorously. A black precipitate has been formed which was left to crystallize for 30 min under stirring. The crystallized product has been then washed with deoxygenated water under magnetic decantation until pH of suspension became below 7.5. The precipitate was dried at room temperature to give a black powder and marked as MGO.

#### Polypyrrole/magnetic graphene oxide preparation

About 5.4 g FeCl<sub>3</sub> added to 100 mL water containing 10 gm of MGO and then the uniform solution was resulted by using a magnetic mixer. After 30 min, 2 mL from freshly distilled pyrrole monomer was added to the stirred aqueous solution. The reaction was carried out for 5 h at room temperature. Consequently, the resulted polymer was filtered on filter paper and to separate the oligomers and impurities, the product was washed several times with deionized water and dried at a temperature of about 60 °C in the oven for 24 h. The obtained GO, MGO, and PPy/MGO composite were characterized by scanning electron microscopy (SEM), Fourier transforms infrared spectroscopy (FT-IR).

#### Characterization

Transmission electron microscopy (TEM) performed on a JEM-2100 (JEOL) transmission electron microscope, FT-IR spectra were measured on a Perkin-Elmer 580B IR spectrophotometer, the specific surface

area was measured by N<sub>2</sub> adsorption-desorption at 77 K on a Quadrasorb SI-MP instrument and Raman spectra

#### Adsorption experiments

Th(IV) adsorption experiments were carried out in closed Erlenmeyer flasks of 50 mL using 0.1g of PPy/MGO and 20 mL of 250ppm Th(NO<sub>3</sub>)<sub>4</sub> solutions, where the pH values were adjusted to the desired values by the addition of 0.1 mol/L HCl or NaOH. The flasks were gently shaken for 45 minutes on Shaker to reach equilibration. The adsorbents and solution were separated by centrifugation and the concentration of Th(IV) in the original solution and left in bulk solution was determined with a spectrophotometer using Thoron (0.1%, w/v) as a chromogenic agent at a wavelength of 540 nm [41]. And for more accuracy, the ICP OS has been used for uranium determination. The adsorption capacity (*q<sub>e</sub>*) and removal efficiency were obtained using the Eqs. (1) and (2):

$$q_e (\mu\text{mol/g}) = \frac{(C_o - C_e)V}{m} \quad (1)$$

$$\text{Removal efficiency (\%)} = \frac{(C_o - C_e)V}{C_o V} \times 100 = \quad (2)$$

$$\left(1 - \frac{C_e}{C_o}\right) \times 100$$

Where *C<sub>o</sub>* and *C<sub>e</sub>* are the Th(IV) ions concentration in the solution initially and at equilibrium (μmol/L), respectively, *V* is the volume of the solution (L), *m* is the weight of adsorbent (g) and *q<sub>e</sub>* is the amount of Th(IV) adsorbed on PPy/MGO at equilibrium (μmol/g).

The adsorption experiments were studied in detail under varying operating conditions, such as the pH value of Th(IV) solutions (1–6), contact time (0–120 min), adsorbent dosage (2–20 mg), the initial Th(IV) concentration (0.042–0.646 mmol/L) and temperature (298–333 K). Furthermore, the pseudo-first-order, pseudo-second-order models were employed to describe the adsorption process. The Langmuir and Freundlich isotherm models were applied to describe the adsorption equilibrium at room temperature. The thermodynamic constants (Δ*H*<sup>o</sup>, Δ*S*<sup>o</sup> and Δ*G*<sup>o</sup>) of the adsorption process were also evaluated. All the experiments have been carried out in duplicate and the averaged values were taken with the standard deviation.

### Samples analysis

Two samples were collected, one from the NMA laboratory waste and the other samples were collected from a geological sample obtained from South Eastern Desert (Abu Resheed area) and complete chemical analysis was carried out. The latter involved the major oxides besides the tenor of the economic metal values. For this purpose, a representative sample portion of the collected technological sample was properly prepared by crushing, grinding to  $-200$  mesh size and quartering. The major oxides were analyzed using the *Shapiro* and *Brannock* [42] rapid silicate analytical procedure. This procedure involves the preparation of two main solutions, namely an alkaline one for  $\text{SiO}_2$  determination and an acid solution for the determination of most of the other oxides like  $\text{Al}_2\text{O}_3$ ,  $\text{CaO}$ ,  $\text{MgO}$ , total iron,  $\text{Na}_2\text{O}$ ,  $\text{K}_2\text{O}$ , etc. Special sample portions were used for the determination of the weight loss at various temperatures to estimate the loss of ignition. These samples subjected to processing and in Table 1 there are two waste lab samples provided from the mentioned original sample after processing.

## 3. RESULTS AND DISCUSSION

### Characterization of the PPy/MGO

#### Fourier transform infrared FTIR spectra of the prepared GO and PPy/MGO

The FTIR spectra for the MGO sheets, PPy, and PPy/GO are shown in Fig. 1. The GO spectrum shows a broad and intense peak centered at  $3385\text{ cm}^{-1}$  and a peak at  $1732\text{ cm}^{-1}$ , are related to the  $-\text{OH}$  groups and the carbonyl ( $\text{C}=\text{O}$ ) stretching, respectively. The peaks at  $1339$ ,  $1223$  and  $1057\text{ cm}^{-1}$  are assigned to the  $\text{O}-\text{H}$  deformation of the carboxyl ( $\text{C}-\text{OH}$ ) and epoxide ( $\text{C}-\text{O}-\text{C}$ ) groups, respectively. The peak at  $1601\text{ cm}^{-1}$  is associated with the remaining  $\text{sp}^2$  character of graphite [43]. In the case of PPy film, the characteristic peaks are located at  $1530\text{ cm}^{-1}$  and  $1447\text{ cm}^{-1}$ , which are due to the anti-symmetric and symmetric ring-stretching modes, respectively [44]. Strong peaks near  $1143\text{ cm}^{-1}$  and  $885\text{ cm}^{-1}$  indicate the doping state of polypyrrole, and broadband at  $3000-3500\text{ cm}^{-1}$  describes  $\text{N}-\text{H}$  and  $\text{C}-\text{H}$  stretching vibrations. Furthermore, the bands at  $1030$  and  $1282\text{ cm}^{-1}$  are attributed to  $\text{C}-\text{H}$  deformation vibrations and  $\text{C}-\text{N}$  stretching vibrations, respectively [45-48]. Compared with the pure PPy, it is clearly observed that

most of the marked peaks are shifted left when the MGO was introduced into the synthesis process of PPy. This reveals that the groups from graphene are associated to the nitrogenous functional groups of PPy backbone via the same doping process into the PPy backbone [49]. Herewith, there probably exist interactions such as  $\pi-\pi$  stacking between polypyrrole backbone and MGO or hydrogen bonding for the residual oxygen functional groups on MGO.

Characteristic peaks of both PPy and MGO can be found in the spectrum of PPy/MGO composite at  $1728$  ( $\text{C}=\text{O}$ ),  $1547$  ( $\text{C}-\text{C}$ ),  $1456$  ( $\text{C}-\text{N}$ ) and  $1042\text{ cm}^{-1}$  ( $\text{C}-\text{H}$ ). However, some of the peaks in the composite have been downshifted, which may be due to the  $\pi-\pi$  stacking between the GO sheets and aromatic pyrrole rings [50]. These results suggest that GO has been successfully incorporated into the PPy film.

### XRD analysis of PPy/MGO

The crystal structure of the prepared samples has been identified by X-ray powder diffraction techniques. As shown in Fig. 2, (GO) intense and sharp peak located at  $2\theta = 10.6^\circ$  is attributed to the (002) crystalline plane of GO and the corresponding interlayer spacing is about  $0.87\text{ nm}$  and this value is larger than the  $d$  spacing ( $0.34\text{ nm}$ ) of pristine graphite ( $2\theta = 26.5^\circ$ ), as a result of the introduction of oxygenated functional groups on the carbon sheets [51-53]. The diffraction peaks of MG composites are consistent with the standard XRD pattern of face-centered cubic (fcc)  $\text{Fe}_3\text{O}_4$ , indicating the coexistence of  $\text{Fe}_3\text{O}_4$  and graphene in the MG composites. Seen from the XRD pattern of the PPy/MGO nanocomposites, all diffraction peaks are similar to that of GF nanocomposites, demonstrating the presence of  $\text{Fe}_3\text{O}_4$  in the composites after polymerization of pyrrole monomers in acid solution also the new peak is situated at  $25^\circ$ , almost the same as that of pure PPy, which was ascribed to the diffraction peak of PPy.

Additionally, the peak ascribed to GO within these nanocomposites disappeared, illustrating the complete coating of PPy between the layered GO [54].

### Raman spectroscopy of PPy/MGO

Raman spectroscopy has been acknowledged as an essential tool for gaining insight into the structural characteristics and properties of carbonaceous materials [55-61].

**Table 1: Chemical analysis of major oxides (wt %) of sample 2.**

Sample no. (%)	SiO <sub>2</sub>	Al <sub>2</sub> O <sub>3</sub>	TiO <sub>2</sub>	P <sub>2</sub> O <sub>5</sub>	Fe <sub>2</sub> O <sub>3</sub>	CaO	MgO	Na <sub>2</sub> O	K <sub>2</sub> O	Loss of Ignition
Sample 1	67.24	12.73	0.028	0.17	4.1	3.7	2.2	4.62	2.9	0.92
Sample 2	63.58	14.06	0.036	0.11	2.4	4.2	4	7.43	2.83	1.33

**Table 2: Chemical specification of the collected waste samples.**

Parameter	NMA waste sample 1 (ppm)	NMA waste sample 2 (ppm)
pH	4.8	3.2
Ca <sup>2+</sup>	1425	2369
Mg <sup>2+</sup>	189	809
Na <sup>+</sup>	67628	52630
K <sup>+</sup>	872	634
Cl <sup>-</sup>	61349.7	82271
CO <sub>3</sub> <sup>2-</sup>	131	99
HCO <sub>3</sub> <sup>-</sup>	1925	1456
SO <sub>4</sub> <sup>-</sup>	3225	6271
Th <sup>4+</sup>	331	77.8
U <sup>6+</sup>	77.8	331
Pb <sup>-</sup>	6.5	9.5
Cr <sup>2+</sup>	8.2	13.7
Co <sup>2+</sup>	16	3
Cu <sup>2+</sup>	8.9	7
Mn <sup>2+</sup>	53.9	11

Fig. 3 shows the Raman spectra of prepared graphite (GF), GO, PPy/MGO in the region of the characteristic D and G bands. In the spectrum of prepared graphite, the peak at 1580 cm<sup>-1</sup> (G band) corresponds to an E<sub>2g</sub> mode of graphite and is related to the vibration of sp<sup>2</sup>-bonded carbon atoms in a 2D hexagonal lattice. The peak at 1350 cm<sup>-1</sup> (D band, the breathing mode of κ-point phonons of A<sub>1g</sub> symmetry) is associated with vibrations of carbon atoms with dangling bonds in plane terminations of disordered graphite. Comparing with raw graphite, the G mode of GO becomes weaker and broader, suggesting a higher level of disorder of the graphene layers and defects increased during the functionalization

process. Besides, the ratio of the intensities (I<sub>D</sub>/I<sub>G</sub>) for GO samples is markedly increased, indicating the formation of some sp<sup>3</sup> carbon by functionalization.

This phenomenon may be attributed to the significant decrease of the size of the in-plane sp<sup>2</sup> domains due to oxidation and ultrasonic exfoliation and partially ordered graphite crystal structure of graphene nanoplatelets. The spectrum shows the D and G bands in the ratio expected for GO and is consistent with data previously reported. As for magnetic nanoparticles, comparing with data in the literature, [62-63].

Upon introducing PPy to GO, a decrease in peak intensity of the D and G bands of the PPy- MGO

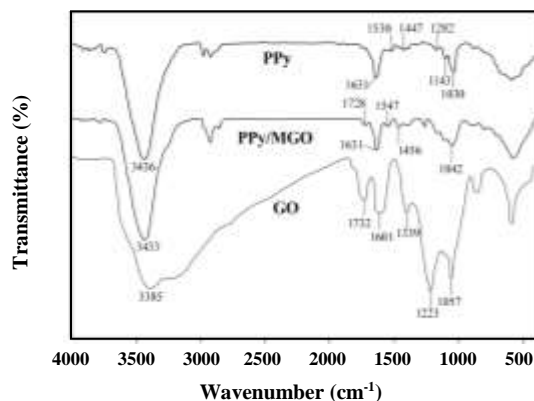


Fig. 1: FTIR spectra of GO, PPy and PPy/MGO.

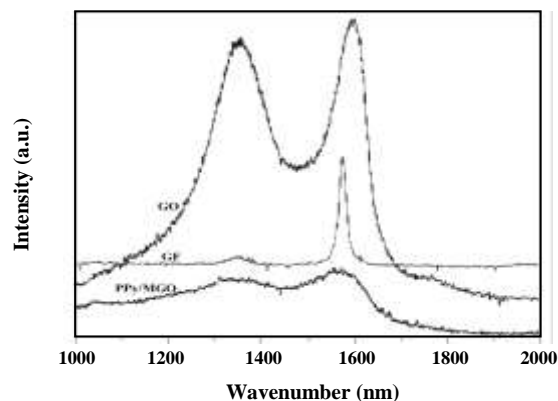


Fig. 3: Raman spectra of graphite (GF), GO and PPy/MGO.

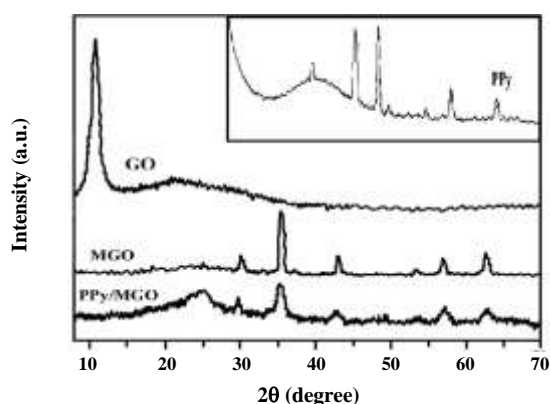


Fig. 2: X-ray diffraction patterns of the pristine graphene oxide (GO), magnetic graphene oxide (MGO), polypyrrole (PPy) and PPy/MGO.

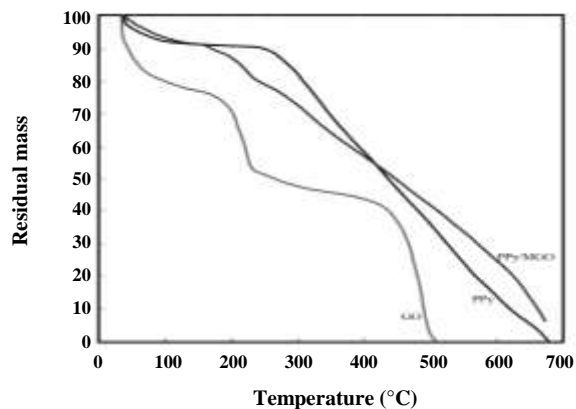


Fig. 4: Thermogravimetric analysis of GO, PPy and PPy/MGO composite.

spectrum is observed, which reveals the p-p interaction between the PPy and the GO sheets [64]. This may be attributed to the presence of localized sp<sup>3</sup> defects within the sp<sup>2</sup> carbon network, which shows a possible agreement with the chemical grafting of polymers to the GO surface [65].

#### Thermogravimetric analysis of PPy/MGO

For further investigation, the thermal stability of the GO, PPy/MGO, and PPy, thermogravimetric measurements has been used; the plotted results in Fig. 4, show typical steps of weight loss for PPy in the air. The pure PPy is stable in the temperature ranging from 30°C to 250°C and shows only about 10% mass loss of residual water. However, a rapid change in mass takes place in the range from 250°C to 670 °C, which corresponds to polymer degradation. As shown in Fig. 3, GO starts

to lose mass upon heating even below 80°C–100°C owing to water between the layers in GO; a second major mass loss occurs at about 210°C, presumably due to pyrolysis of oxygen-containing functional groups such as COOH and COH, yielding CO<sub>2</sub>, CO, and water [66, 67]. Another mass loss happens at about 490°C because of carbon combustion [68]. In the case of the PPy/MGO composite in Fig. 4, the first small section of weight loss from 30°C to 100°C arises mainly because of the expulsion of absorbed water and the free acid in the PPy. The second step for weight loss, at about 200°C, is due to pyrolysis of COOH and COH. However, more mass remains for the PPy/MGO composites than the pure PPy at temperatures greater than 420°C due to the existence of a carbon net structure, which can improve thermal stability and effectively reduce the decomposition rate of PPy/MGO above 420°C.

### EDX pattern of PPy/MGO composite

Fig. 5 shows the typical EDX pattern of nanoparticle PPy/MGO before and after thorium adsorption which indicates the appearance of two peaks of 3.2 and 3.9 keV as a result of adsorption of thorium on the surface of PPy/MGO composite.

### Factor affecting the adsorption of thorium on the surface of PPy/MGO

#### Effect of pH

The solution pH is thought to be a significant factor affecting the metal ions sorption on the sorbent because it obviously influences the species of metal ions together with the surface charge and the active sites of the sorbent in the solution

Fig. 5 shows the effect of pH on the adsorption of Th(IV) on PPy/MGO, The removal efficiency of Th(IV) increased sharply with an increase of pH from 1 to 4 and got a maximum value at pH 4.5 and being constant after that but from pH 4.5 white precipitate formed from thorium so that these results after pH are excluded [68].

The adsorption efficiency of Th(IV) is low at pH value below 1–3 due to the protonation of residual oxygen-containing groups on PPy/MGO (such as hydroxyl group) and the competition between  $H^+$  and Th(IV) ions for the same adsorption site [69-71]. It should be noted that thorium ions may convert to hydroxide complexes at high pH value, the main species is Th(IV) at pH 4.0 and  $Th(OH)_2^{2+}$  at pH 4.5 [72]. Hence, pH 4.0 for Th(IV) adsorption was selected in the following studies. The pH value is limited within 4 in case of a soluble form of Th(IV) ions due to these ions will be converted into insoluble species according to solubility calculations [48].

It is well known that Th(IV) can easily form precipitation at  $pH > 4$  because of the low solubility of  $Th(OH)_4$  ( $K_{sp}=2.0 \times 10^{-45}$ ). At  $pH < 4$ , the adsorption percent of Th(IV) reaches to about 92%, so the removal of Th(IV) from solution to PPy/MGO is not attributed to the precipitation [73]. The results of thorium sorption on PPy/MGO are a quite strong surface complexation rather than cation exchange contributes mainly to thorium sorption.  $Th^{4+}$  and  $Th(OH)^{3+}$  are the main species and each contributes 50%; at  $pH < 4$ ,  $Th^{4+}$  and  $Th(OH)^{3+}$  are the predominating species. The species of Th(IV) as a function of pH values are shown in Fig. 7 according to Moulin, C., et al. [74].

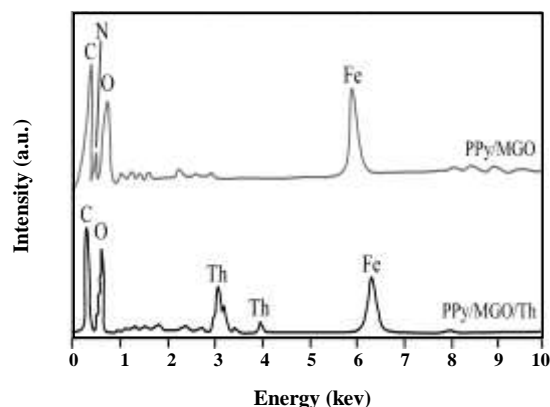


Fig. 5: EDX pattern of PPy/MGO before and after thorium adsorption.

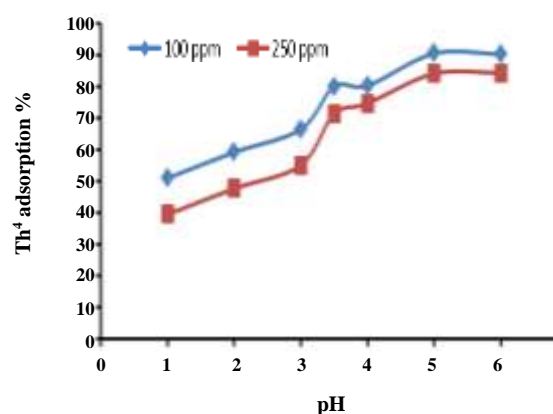


Fig. 6: Effect of solution pH on Th(IV) adsorption efficiency on PPy/MGO using two different concentration (100 and 250 ppm, room temperature, 30min. contact time, 0.1 gm composite, 20 ml sample).

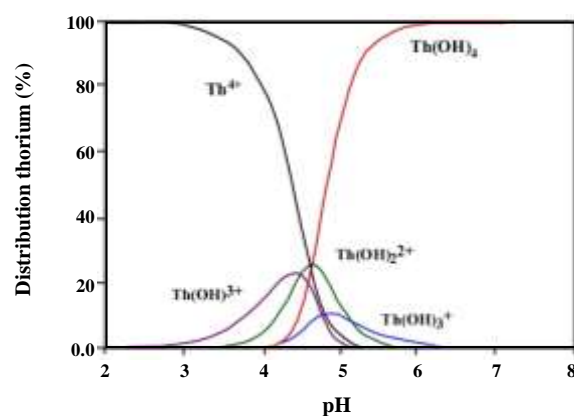


Fig. 7: Chemical Speciation of Thorium after Moulin, C., et al. [74].

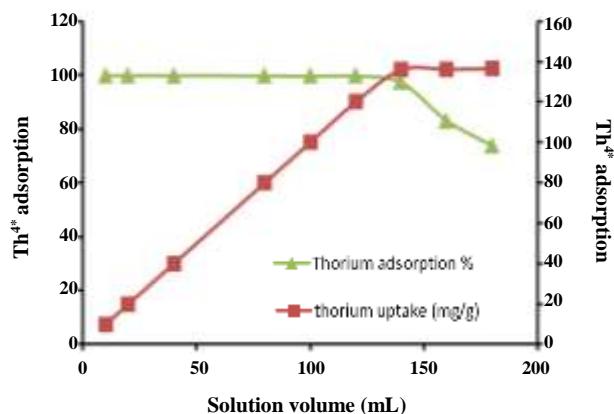


Fig. 8: Effect of adsorbent dosage on the adsorption of Th(IV) on PPy/MGO. (pH 4, 20 mL sample, room temperature, 20 min contact time)

The main problem here is that Th forms very insoluble hydroxides even at low pH. In this regard, low concentration of thorium does not reach 500 mg/L and no additive as oxalate helps thorium to still soluble at all the different pH. With respect to thorium hydroxide precipitation has been applied only at pH 7.

#### Sorbent Dosage

The effect of adsorbent dosage on the adsorption of Th(IV) on PPy/MGO is studied in the range from 0.1 to 0.5 gm of sorbent dosage. As shown in Fig. 8, the adsorption capacity of Th(IV) decreased with the increase of the adsorbent dosage from 0.2 up to 0.5 gm [45,46]. When the adsorbent dosage is higher than 0.1 g, the adsorption capacity of Th(IV) on PPy/MGO is not significantly altered and due to the increase of the dose with the same constant concentration of Th (IV) on the medium. So, 0.1 gm of PPy/MGO is chosen for the subsequent experiments.

#### Effect of contact time

The effect of contact time on the adsorption of Th(IV) studied on the range from 5 to 60 minutes was plotted in Fig. 9. The adsorption was rapid at first and then reached equilibrium within 30 min. The short equilibrium time indicates high efficiency and economic feasibility of the sorbent for industrial applications.

In order to investigate the controlling mechanism of the adsorption process, the pseudo-first-order and pseudo-second-order kinetic models are used to evaluate the experimental data obtained from batch Th(IV) removal

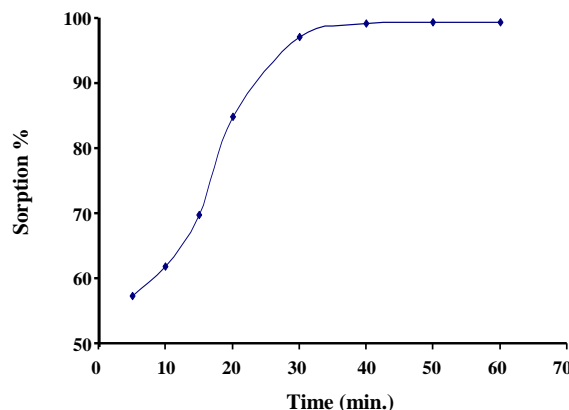


Fig. 9: Effect of contact time on the Th(IV) adsorption. (pH 4, 20ml sample, room temperature, 0.1 gm. sorbent dosage).

experiments. Pseudo-first-order kinetic model and pseudo-second-order kinetic model are shown in Eqs. (3) and (4) [33].

$$\text{Pseudo - first - order : } \ln(q_e - q_t) = \ln q_e - k_1 t \quad (3)$$

$$\text{Pseudo - second - order : } t/q_t = 1/k_2 q_e^2 + 1/q_e t \quad (4)$$

Where  $q_e$  and  $q_t$  are the amounts of Th(IV) adsorbed (mg/g) at equilibrium and at time  $t$  (min), respectively.  $k_1$  ( $\text{min}^{-1}$ ) and  $k_2$  ( $\text{g/mg/min}$ ) are the rate constants of pseudo-first-order and pseudo-second-order rate constants, respectively.

Kinetic parameters are calculated and shown in Table 3 and (Figs. 10 and 11). Results clearly indicate that the rate of adsorption of Th(IV) onto PPy/MGO composite depends on the initial concentration of Th(IV). The applicability of these models was quantified from the coefficient of determination,  $R^2$  values. The values of  $R^2$  show that the pseudo-second-order can describe the experimental data better than the pseudo-first-order model. Moreover, the theoretical  $q_e$  values calculated from the pseudo-second-order model are close to the experimental data. These results confirm the validity of the pseudo-second-order model to the adsorption system, suggesting the main adsorption mechanism of chemical adsorption.

#### Effect of Initial thorium concentration

The effect of initial thorium concentration was studied by using a range of initial thorium concentrations between 50 and 3000 mg/L at three fixed temperatures (298, 323 and 333 K). As shown in Fig.12, the Th(IV)

Table 3: Pseudo-first and second order model parameters of Th(IV) sorption onto PPy/MGO.

First ordered Kinetic				2nd ordered Kinetic		
$K_1$	$Q_{\max}(\text{cal})$	$r^2$	$Q_{\max}(\text{exp})$	$K_2$	$Q_{\max}(\text{cal})$	$r^2$
0.114	27.31	0.8117	24.9	0.007	25.19	0.9931

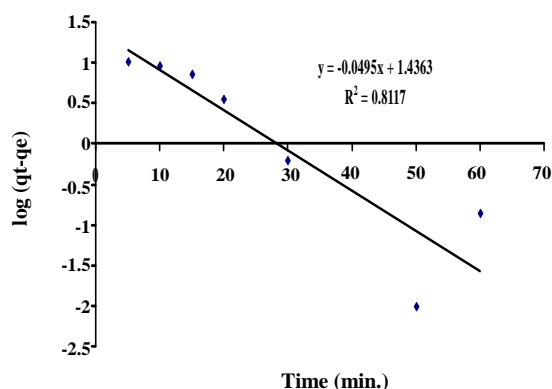


Fig. 10: First order kinetics plot for the adsorption of Th (IV) onto PPy/MGO composite. (pH 4, 20 mL sample, room temperature, 0.1 gm. sorbent dosage).

uptake capacity increase with the increase in the initial thorium concentration. This may be due to higher metal ion concentration-enhancing the driving force to overcome mass transfer resistance between the aqueous and solid phases [75]. Further, it is observed that the temperature has a slightly positive effect on the adsorption of thorium using PPy/MGO indicating that the process to be endothermic in nature.

### Sorption isotherms

The sorption isotherms of Th(IV) ions on PPy/MGO composite are shown in Figs. 12, 13. In order to better understand the sorption mechanism, the experimental data are simulated by the Langmuir and the Freundlich models [47]. The Langmuir model assumes that the surface and bulk phases of homogeneous sorbents are of ideal behavior and has been widely used to describe the monolayer sorption process. It is expressed as:

$$\frac{C_e}{q_e} = \frac{1}{b \cdot Q_{\max}} + \frac{C_e}{Q_{\max}} \quad (5)$$

Where  $Q_{\max}$  (in milligrams per gram) represents the maximum amount of metal ions per unit weight of adsorbent to form a complete monolayer on the surface,  $b$  is the equilibrium adsorption constant or Langmuir

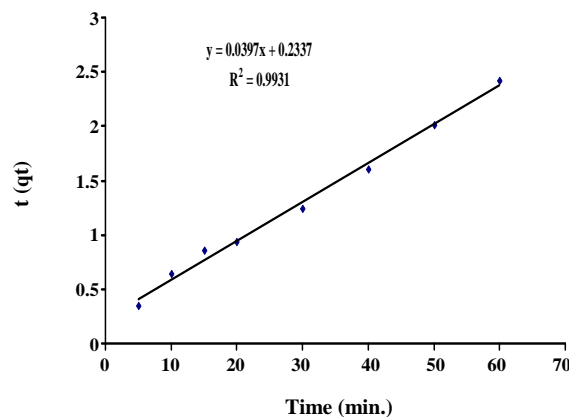


Fig. 11: Second order kinetics plot for the adsorption of Th (IV) onto PPy/MGO composite. (pH 4, 20 mL sample, room temperature, 0.1 gm. sorbent dosage).

sorption coefficient that represents enthalpy of sorption,  $q_e$  is the number of metal ions adsorbed by adsorbent at equilibrium, and  $C_e$  is the equilibrium concentration of thorium ions.

The linearized Freundlich model is:

$$\ln q_e = \ln k + \left(\frac{1}{n}\right) \ln C_e \quad (6)$$

Where  $1/n$  is an indicator of isotherm nonlinearity corresponding to the sorption intensity at a particular temperature and  $k$  ( $\text{mg}^{1-n} \text{L}^n \text{g}^{-1}$ ) is the Freundlich sorption coefficient related to the sorption capacity of PPy/MGO.

The linear dependency of the Langmuir model and the Freundlich model of Th(IV) sorption on PPy/MGO composite is shown in Figs. 13 and 14. The relative parameters are listed in Table 4.

Although the correlation coefficient  $R^2$  of Freundlich isotherm is higher than Langmuir isotherm but the theoretical uptake obtained from Langmuir is so close to experimental uptake which means that Langmuir isotherm shows a better fitting model compared to Freundlich isotherm. The high correlation coefficient of Langmuir isotherm indicates that Th(IV) ions strongly adsorbed to the surface of PPy/MGO composites

**Table 4: Parameters of Langmuir and Freundlich models of Th(IV) sorption on PPy/MGO composite.**

Langmuir isotherm				Freundlich isotherm			
Temp. °C	b	q <sub>m</sub>	R <sup>2</sup>	q <sub>t</sub>	K <sub>f</sub>	1/n	R <sup>2</sup>
25	0.0075	270.27	0.8971	256.5	3.245	0.4145	0.9907
50	0.0086	273.16	0.8788	261.09	2.884	0.4968	0.9921
60	0.0179	277.8	0.8871	264.98	2.881	0.5066	0.9905

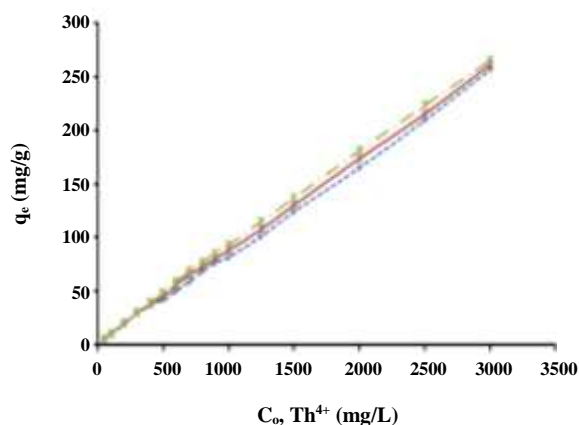


**Fig. 12: Effect of initial thorium concentration on Th(IV) adsorption efficiency onto PPy/MGO composite. (pH 4, 20mL sample, room temperature, 0.1 gm. sorbent dosage and 30 min contact time).**

and the adsorption is monolayer adsorption. It is verified that PPy/MGO has great potential to be a good adsorbent for the removal of thorium ions.

As an important parameter of sorbents, excellent dispersion can extend the number of binding sites in aqueous solutions.

The diffusion property of PPy/MGO composites is much better than that of PPy polymers. This is attributed to the nitrogen and oxygen-containing functional groups on the surfaces of PPy/MGO composites, which reduces the aggregation of PPy/MGO particles caused by van der Waals forces. A much smaller particle size provides a much higher specific surface area, resulting in the higher sorption capacity of PPy/MGO composites than that of PPy polymers. Besides the large surface area and excellent dispersion property, it is reasonable that the functional groups, especially the nitrogen-containing groups, can form strong complexes with Th(IV) ions [76-77]. All these results clearly indicate that PPy/MGO composites are suitable and promising materials in the preconcentration and removal of Th(IV) ions from aqueous solutions.

The degree of suitability of the adsorbent towards metal ions was estimated from the values of separation factor constant ( $R_L$ ) (equation 7) which gave indication for the possibility of the adsorption process to proceed as follow:  $R_L > 1$  unsuitable;  $R_L = 1$  linear;  $0 < R_L < 1$  suitable;  $R_L = 0$  irreversible.

The values of  $R_L$  lie between 0.727 and 0.0425 which indicate the suitability of the adsorbent for Th(IV) from aqueous solution.

Also, the observed increase in  $K_L$  values with temperature indicates that the adsorption reaction has endothermic nature. This can be confirmed by the calculation of the thermodynamic parameters.

$$R_L = 1/(1 + K_L C_o) \quad (7)$$

$$\ln K_L = \frac{-\Delta H^\circ}{RT} + \frac{-\Delta S^\circ}{R} \quad (8)$$

$$\Delta G^\circ = \Delta H^\circ - T\Delta S^\circ \quad (9)$$

Thermodynamic parameters ( $\Delta H^\circ$ ,  $\Delta S^\circ$ , and  $\Delta G^\circ$ ) were calculated from the equations listed previously and their values were tabulated in Table 5. The obtained results show that the increase in the negative values of  $\Delta G^\circ$  with increasing temperature gives an indication that the adsorption process became more favorable at a higher temperature. At all studied temperature the values of  $|\Delta H^\circ| < |T\Delta S^\circ|$ . This indicated that the adsorption process was dominated by entropic rather than enthalpic changes. The positive values of  $\Delta H^\circ$  indicate that the reaction was an endothermic adsorption process. The positive value of  $\Delta S^\circ$  could be explained by the increased degree of randomness.

#### Elution efficiency

The desorption experiments of Th(IV) ions are carried out by rinsing the PPy/MGO composites adsorbed Th(IV) ions with a series of concentrations (0.001, 0.01, 0.1, 0.5, 1.0 M) of HCl and HNO<sub>3</sub> solutions for 6 h under

**Table 5: Thermodynamic parameters for adsorption of Th(IV) on composite at different temperatures.**

$\Delta H^\circ$ (kJ/mol)	$\Delta S^\circ$ (J/mol K)	$\Delta G^\circ$ (kJ/mol)		
		298 K	323 K	333 K
825.01	37.81	-10.44	-11.39	-11.77

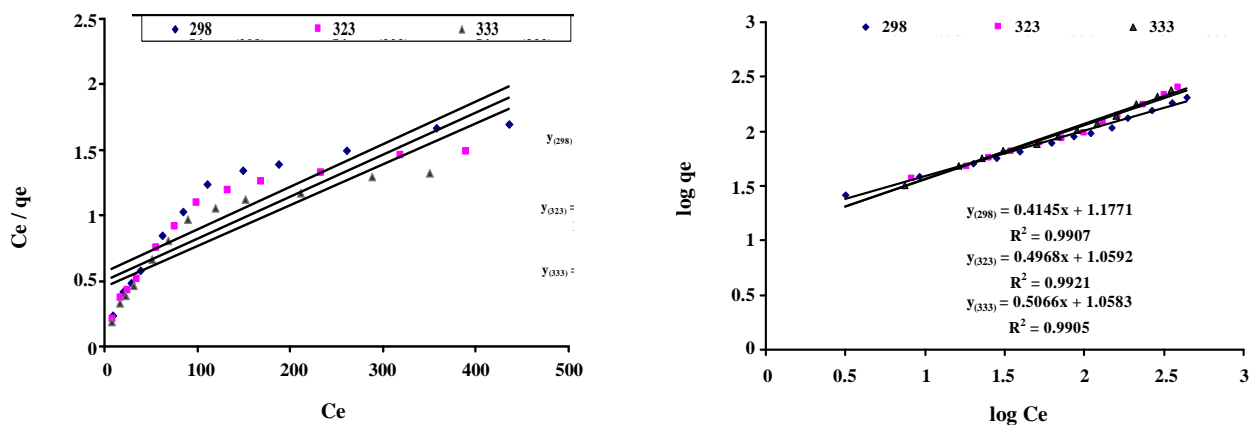


**Fig. 13: (a) Langmuir isotherms and of Th(IV) ions on PPy/MGO composites. (pH 4, 20 mL sample, room temperature, 0.1 gm. sorbent dosage and 30 min contact time). (b) Freundlich isotherms and of Th(IV) ions on PPy/MGO composites. (pH 4, 20 mL sample, room temperature, 0.1 gm. sorbent dosage and 30 min contact time).**

continuous stirring Fig. 14. Then the composite separated by centrifugation and the concentrations of Th (IV) in solutions determined with UV Vis spectrophotometer using Thorin as a reagent. The experimental results show that 1M HCl solution is the best eluent giving the best efficiency in comparison with the other concentrations, indicating that PPy/MGO composites have a good desorption property for Th(IV) ions under 1.0 M HCl solution, which is suitable for the reusability of the PPy/MGO composites in real possible applications.

The chemical stability of PPy/MGO in acid and alkaline media was tested by shaking a 0.5 g portion of the composite in turn with 100mL of 1M HCl and 1M NaOH for 24h. The composite was then filtered off and washed with water. The adsorption capacities after the treatments were reduced by only 5–7%, which were denoted as desirable stability of the composite. No obvious change of composite was observed in the experimental process.

The reusability through sorption-desorption cycles for heavy metal ions and radionuclides is a key factor for applications of sorbents with long-term performance. The above results indicate that the PPy/MGO composites can be regenerated very well with 1.0 M HCl solution.

The recycling times of PPy/MGO composites for the removal of Th(IV) ions are also investigated. As shown in Fig.15, the concentration of HCl solution used for desorption was chosen to be 1.0 M after Th(IV) sorption. The suspension of PPy/MGO composites is shaken for 6h, separated by centrifugation. this experiment also displays that the adsorption capacity could maintain above 90 % of its initial capability after three cycles and above 80 % after three cycles. The result here illustrates that PPy/MGO composites have high stability and can be used as regenerated availability adsorbents in the preconcentration and sorption of Th(IV) ions from aqueous solutions in possible real applications.

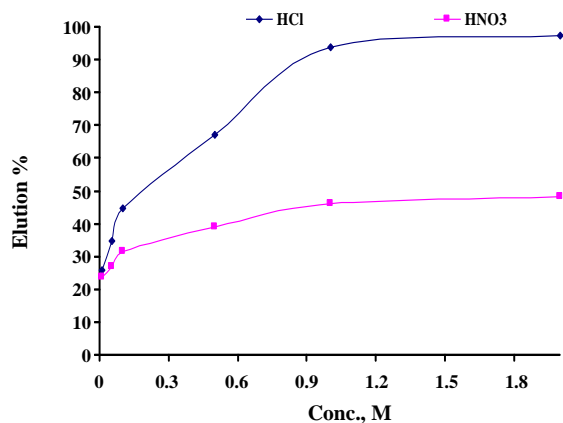
#### **Application on the NMA laboratories wastewater**

To investigate the applicability of the prepared PPy/MGO composites to remove Th(IV) contaminant from wastewater samples obtained from NMA laboratories, and the geological sample collected from the southeastern desert (sample 2).

The application of the adsorption carried on under fixed conditions; contact time 30 min, pH 4 and at 60 °C temperature. 20 mL solution is contacted with 0.1g from the PPy/MGO, after equilibration, the solution filtered

Table 6: Effect of PPy/MGO on the thorium concentration of the collected samples.

	NMA waste sample 1	Sample 2
Th <sup>4+</sup> conc. before treatment with PPy/MGO	77.8	331
After treatment	Under detection limit	Under detection limit

Fig. 14: Effect of HCl and HNO<sub>3</sub> concentration on elution of Th(IV) loaded on PPy/MGO composites.

and analyzed for the thorium concentration and it is found that nearly all the thorium ions have been adsorbed on the PPy/MGO. From the obtained data (Tables 6), it is clear that the prepared PPy/MGO is efficient in thorium removal from waste effluents with efficiency exceed 99.99%.

## CONCLUSION

PPy/MGO is used to modify GO surface successfully by polymerization technique. The batch adsorption results demonstrated that PPy/MGO composites present excellent Th(IV) adsorption properties from aqueous solutions. The adsorption of Th(IV) from aqueous solutions onto PPy/MGO composites is pH dependent whereas independent of competitive cations. Due to the unique and tunable physicochemical properties, such as (a) high selectivity for trace level Th(IV), (b) excellent stability in aqueous solutions, and (c) easily regenerated with a simple and environment-friendly method, PPy/MGO composites can be used as promising adsorbents for the preconcentration and extraction of Th(IV) from aqueous solution, wastewater and from geologic samples.

Received: Jul. 18, 2016 ; Accepted: Sep. 20, 2017

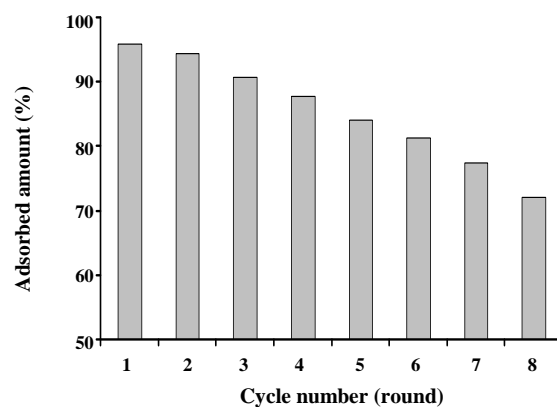


Fig. 15: Recycling of PPy/MGO composites for the removal of Th(IV) ions.

## REFERENCES

- [1] Brugge D., deLemos J.L., Oldmixon B., [Exposure Pathways and Health Effects Associated with Chemical and Radiological Toxicity of Natural Uranium: A Review](#), *Rev. Environ. Health*, **20**: 177- (2005).
- [2] Metwally E., [Kinetic Studies for Sorption of Some Metal Ions From Aqueous Acid Solutions onto TDA Impregnated Resin](#), *J. Radional. Nucl. Chem.*, **270**: 559-566 (2006).
- [3] Sharma P., Tomar R., [Synthesis and Application of an Analogue of Mesolite for the Removal of Uranium\(VI\), Thorium\(IV\), and Europium\(III\) From Aqueous Waste](#), *Microporous Mesoporous Mater*, **116**: 641-652 (2008).
- [4] Tang Y.Z., Reeder R.J., [Uranyl and Arsenate Cosorption on Aluminum Oxide Surface](#), *Geochim. Cosmochim. Acta*, **73**: 2727-2743 (2009).
- [5] Shao D.D., Li J.X., Wang X.K., [Poly\(amidoxime\)-Reduced Graphene Oxide Composites as Adsorbents for the Enrichment of Uranium from Seawater](#), *Sci. China Chem.*, **57**: 1449-1458 (2014).
- [6] Gado M., Morsy A., [Preparation of Poly-Aniline-Magnetic Porous Carbon Composite for Using as Uranium Adsorbent](#), *American Journal of Materials Synthesis and Processing*, **2**: 32-40 (2017).

- [7] Olmez Aytas S., Akyil S., Eral M., [Adsorption and Thermodynamic Behavior of Uranium on Natural Zeolite](#), *J. Radioanal. Nucl. Chem.*, **260**: 119-125 (2004).
- [8] Shahwan T., Erten H.N., [Characterization of Sr<sup>2+</sup> Uptake on Natural Minerals of Kaolinite and Magnetite Using XRPD SEM/EDS, and DRIFT](#), *Radiochim. Acta*, **93**: 225- (2005).
- [9] Shehata F.A., Attallah M.F., Borai E.H., Hilal M.A., Abo-Aly M.M., [Sorption Reaction Mechanism of Some Hazardous Radionuclides From Mixed Waste by Impregnated Crown Ether onto Polymeric Resin](#), *Appl. Radiat. Isot.*, **68**: 239-249 (2010).
- [10] Atia A.A., [Studies on the Interaction of Mercury\(II\) and Uranyl with Modified Chitosan Resins](#), *Hydrometallurgy*, **80**: 13-22 (2005).
- [11] Li W.J., Tao Z.Y., [Comparative Study on Th\(IV\) Sorption on Alumina and Silica From Aqueous Solutions](#), *J. Radioanal. Nucl. Chem.*, **254**: 187- (2002).
- [12] Seko N., Tamada M., Yoshii F., [Current Status of Adsorbent for Metal Ions with Radiation Grafting and Crosslinking Techniques](#), *Nucl. Instrum. Methods Phys. Res. Sect. B* **236**: 21-29 (2005).
- [13] Vivero-Escoto J.L., Carboni M., Abney C.W., DeKrafft K.E., Lin, [Organofunctionalized Mesoporous Silicas for Efficient Uranium Extraction](#), *Microporous Mesoporous Mater.*, **180**: 22-31 (2013).
- [14] Prasada Rao T., Metilda P., Mary Gladis J., [Preconcentration Techniques for Uranium\(VI\) and Thorium\(IV\) Prior to Analytical Determination - An Overview](#), *Talanta*, **68**: 1047-1064 (2006).
- [15] Prabhakaran D., Subramanian M.S., [Selective Extraction of U\(VI\) Th\(IV\), and La\(III\) From Acidic Matrix Solutions and Environmental Samples Using Chemically Modified Amberlite XAD-16 Resin](#), *Anal. Bioanal. Chem.*, **379**: 519-525 (2004).
- [16] Donat R., Esen K., Cetisli H., Aytas S., [Adsorption of Uranium\(VI\) onto Ulva sp.-Sepiolite Composite](#), *J. Radioanal Nucl Chem*, **279**: 253- (2008).
- [17] Ilton E.S., Wang Z.M., Boily J.F., Qafoku O., Rosso K.M., Smith S.C., [The Effect of pH and Time on the Extractability and Speciation of Uranium \(VI\) Sorbed to SiO<sub>2</sub>](#), *Environ. Sci. Technol.*, **46**: 6604-6611 (2012).
- [18] Ims S., Ek S., Ulusoy U., [Uranium and Lead Adsorption onto Bentonite and Zeolite Modified with Polyacrylamidoxime](#), *J. Radioanal Nucl. Chem.*, **292**: 41- (2012).
- [19] Belgacem A., Rebiai R., Hadoun H., Khemaissia S., Belmedani M., [The Removal of Uranium \(VI\) From Aqueous Solutions onto Activated Carbon Developed from Grinded Used Tire](#), *Environ. Sci. Pollut. Res.*, **21**: 684-694 (2014).
- [20] Schierz A., Za'anker H., [Aqueous Suspensions of Carbon Nanotubes: Surface Oxidation, Colloidal Stability and Uranium Sorption](#), *Environ. Pollut.*, **157**: 1088-1094 (2009).
- [21] Li Z.J., Chen F., Yuan L.Y., Liu Y.L., Zhao Y.L., Chai Z.F., Shi W.Q., [Uranium \(VI\) Adsorption on Graphene Oxide Nanosheets From Aqueous Solutions](#), *Chem. Eng. J.*, **210**: 539-546 (2012).
- [22] Su Q., Pang S., Alijani V., Li C., Feng X., Müllen K., [Composites of Graphene with Large Aromatic Molecules](#), *Adv. Mater.*, **21**: 3191-3195 (2009).
- [23] Zhao G., Li J., Ren X., Chen C., Wang X., [Few-Layered Graphene Oxide Nanosheets as Superior Sorbents for Heavy Metal Ion Pollution Management](#), *Environ. Sci. Technol.*, **25**: 10454-10462 (2011).
- [24] Li D., MU M., Je S.G., Kaner R.B., Wallace G., [Processable Aqueous Dispersions of Graphene Nanosheets](#), *Nat. Nanotechnol.*, **3**: 101-105 (2008).
- [25] Yuan W., Shi G., [Graphene-Based Gas Sensors](#), *J. Mater. Chem. A.*, **1**: 10078- (2013).
- [26] Harshal P., Mungse H.P., Sharma O.P., Hiroyuki Sugimura H., Khatri O.P., [Hydrothermal Deoxygenation of Graphene Oxide in Sub- and Supercritical Water](#), *J. Mater. Chem.*, **4**: 22589- (2014).
- [27] Konwer S., Boruah R., Dolui S.K., [Studies on Conducting Polypyrrole/Graphene Oxide Composites as Supercapacitor Electrode](#), *J. Electron Mater.*, **40**: 2248- (2011).
- [28] Zhang S., Hao Y.Y., Liu J., Aksay I.A., Lin Y.H., [Graphene-Polypyrrole Nanocomposite as a Highly Efficient and Low Cost Electrically Switched Ion Exchanger for Removing ClO<sub>4</sub><sup>-</sup> From Wastewater](#), *ACS Appl Mater Interf.*, **3**: 3633-3637 (2011).
- [29] Zhu Y., Murali S., Cai W., Li X., Suk J.W., Potts J.R., Ruoff R.S., [Graphene and Graphene Oxide: Synthesis, Properties, and Applications](#), *Advanced Materials*, **22**: 3906- (2010).

- [30] Huang X., Yin Z., Wu S., Qi X., He Q., Zhang Q., Yan Q., Boey F., Zhang H., **Graphene-based Materials: Synthesis, Characterization, Properties, and Applications**, *Small*, **7**: 1876- (2011).
- [31] Liu Y., Dong X., Chen P., **Biological and Chemical Sensors Based on Graphene Materials**, *Chemical Society Reviews*, **41**: 2283- (2012).
- [32] Machado B.F., Serp P., **Graphene-based Materials for Catalysis**, *Catalysis Science & Technology*, **2**: 54- (2012).
- [33] Sharma P., Tomar R., **Synthesis and Application of an Analogue of Mesolite for the Removal of Uranium(VI), Thorium(IV), and Europium(III) from Aqueous Waste**, *Microporous Mesoporous Mater.*, **116**: 641-652 (2008).
- [34] Mowafy E.A., Aly H.F., **Extraction Behaviours of Nd(III), Eu(III) La(III), Am(III), and U(VI) with Some Substituted Malonamides from Nitrate Medium**, *Solvent Extr. Ion Exch.*, **20**: 177- (2002).
- [35] Condamines N., Musikas C., **The Extraction by N,N-Dialkylamides. II. Extraction of Actinide Cations**, *Solvent Extr. Ion Exch.*, **10**: 69-100 (1992).
- [36] Ardois C., Musikas C., Fattahi M., Abbe A.C., **Selective Actinide Solvent Extraction Used in Conjunction with Liquid Scintillation**, *J. Radioanal. Nucl. Chem.*, **226**: 241- (1992).
- [37] Zhen X., Chao G., **In Situ Polymerization Approach to Graphene-Reinforced nylon-6 Composites**, *Macromolecules*, **43**: 6716-6723 (2010).
- [38] Guobo H., Suqing C., Pingan S., Pingping L., Chenglin W., Huading L., **Combination Effects of Graphene and Layered Double Hydroxides on Intumescent Flame-Retardant Poly (methyl methacrylate) Nanocomposites**, *Appl. Clay Sci.*, **88-89**: 78-85 (2014).
- [39] Chenlu B., Lei S., Weiyi X., Bihe Y., Charles A.W., Jianliu H., Yuqiang G., Yuan H., **Preparation of Graphene by Pressurized Oxidation and Multiplex Reduction and Its Polymer Nanocomposites by Masterbatch-Based Melt Blending**, *J. Mater. Chem.*, **22**: 6088-6096 (2012).
- [40] Massart R., **Preparation of Aqueous Magnetic Liquids in Alkaline and Acidic Media**, *IEEE Trans Magn.*, **17**: 1247- (1981).
- [41] Yao J., Sun Y., Yang M., Duan Y., **Chemistry, Physics and Biology of Graphene-Based Nanomaterials: New Horizons for Sensing, Imaging and Medicine**, *Journal of Materials Chemistry*, **22**: 14313-14329 (2012).
- [42] Shapiro, L., Brannock N.W., "Rapid Analysis of Silicate, Carbonate and Phosphate Rocks", U.S. Geo. Surv., Bull, V. 1144, 56 p (1962).
- [43] Chen C., Wang X., **Sorption of Th (IV) to Silica as a Function of pH, Humic/Fulvic Acid, Ionic Strength, Electrolyte Type**, *Applied Radiation and Isotopes*, **65**: 155-163 (2007).
- [44] Gado M., Zaki S., **Studies on Thorium Adsorption Characteristics upon Activated Titanium Hydroxide Prepared from Rosetta Ilmenite Concentrate**, *Int. J. Waste Resources*, **6**: 1000194- (2015).
- [45] Yang X., Xu M.S., Qiu W.M., Chen X.Q., Deng M., Zhang J.L., Iwai H., Watanabe E., Chen H.Z., **Graphene Uniformly Decorated with Gold Nanodots: in Situ Synthesis, Enhanced Dispersibility and Its Applications**, *J. Mater. Chem.*, **21**: 8096- (2011).
- [46] Cho G., Fung B.M., Glatzhofer D.T., Lee J.S., Shul Y.G., **Preparation and Characterization of Polypyrrole-Coated Nanosized Novel Ceramics**, *Langmuir*, **17**: 456-461 (2001).
- [47] Tian B., Zerbi G., **Lattice Dynamics and Vibrational Spectra of Polypyrrole**, *J. Chem. Phys.*, **92**: 3886- (1990).
- [48] Mahmud H.N.M.E., Kassim A., Zainal Z., Yunus W.M.M., **Fourier Transform Infrared Study of Polypyrrole-Poly(vinyl alcohol) Conducting Polymer Composite Films: Evidence of Film Formation and Characterization**, *J. Appl. Polym. Sci.*, **100**: 4107- (2006).
- [49] Zhang X.T., Zhang J., Liu Z.F., Robinson C., **Enhanced Capacitance and Rate Capability of Graphene/Polypyrrole Composite as Electrode Material for Supercapacitors**, *J. Power Sources*, **196**: 1852- (2004).
- [50] Wang H.L., Hao Q.L., Yang X.J., Lu L.D., Wang X., **Graphene Oxide Doped Polyaniline for Supercapacitors**, *Electrochem. Commun.*, **11**: 1158-1161 (2009).
- [51] Bissessur R., Liu P.K.Y., Scully S.F., **Intercalation of Polypyrrole Into Graphite Oxide**, *Synth. Met.*, **156**: 1023-1027 (2006).

- [52] Fan W., Gao W., Zhang C., Tjiu W.W., Pan J.S., Liu T.X., Self-Assembly of Hierarchical Fe<sub>3</sub>O<sub>4</sub> Microsphere/Graphene Nanosheet Composite: Towards a Promising High-Performance Anode for Li-Ion Batteries, *J. Mater. Chem.*, **22**: 25108- (2012).
- [53] Guo H.L., Wang X.F., Qian Q.Y., Wang F.B., Xia X.H., A Green Approach to the Synthesis of Graphene Nanosheets, *ACS Nano*, **3**: 2653-2659 (2009).
- [54] Xu J., Wang K., Zu S.-Z., Han B.-H., Wei Z., Hierarchical Nanocomposites of Polyaniline Nanowire Arrays on Graphene Oxide Sheets with Synergistic Effect for Energy Storage, *ACS Nano*, **4**: 5019-5026 (2010).
- [55] Deng X., Lü L., Li H., Luo F., The Adsorption Properties of Pb(II) and Cd(II) on Functionalized Graphene Prepared by Electrolysis Method, *J. Hazard. Mater.*, **183**: 923-930 (2010).
- [56] Li Y., Zhang P., Du Q., Peng X., Liu T., Wang Z., Xia Z., Zhang W., Wang K., Zhu H., Wu D., Adsorption of Fluoride from Aqueous Solution by Graphene, *J. Coll. Interf. Sci.*, **363**: 348-354 (2011).
- [57] Yang S.T., Chen S., Chang Y., Cao A., Liu Y., Wang H., Removal of Methylene Blue from Aqueous Solution by Graphene Oxide, *J. Coll. Interf. Sci.*, **359**: 24- (2011).
- [58] Bhaumik M., Leswif T.Y., Maity A., Srinivasu V.V., Onyango M.S., Removal of Fluoride from Aqueous Solution by Polypyrrole/Fe<sub>3</sub>O<sub>4</sub> Magnetic Nanocomposite, *J. Hazard. Mater.*, **186**: 150-159 (2011).
- [59] Ballav N., Mishra S., Maity A., High Efficient Removal of Chromium(VI) Using Glycine Doped Polypyrrole Adsorbent from Aqueous Solution, *Chem. Eng. J.*, **198-199**: 536-546 (2012).
- [60] Bao Q., Zhang D., Qi P., Synthesis and Characterization of Silver Nanoparticle and Graphene Oxide Nanosheet Composites as a Bactericidal Agent for Water Disinfection, *J. Coll. Interf. Sci.*, **360**: 463-470 (2011).
- [61] De Faria D.L.A., Silva S.V., de Oliveira M.T., Raman Microspectroscopy of Some iron Oxides and Oxyhydroxides, *J. Raman Spectrosc.*, **28**: 873- (1997).
- [62] Bersani D., Lottici P.P., Montenero A., Micro-Raman Investigation of Iron Oxide Films and Powders Produced by Sol-Gel Syntheses, *J. Raman Spectrosc.*, **30**: 355- (1999).
- [63] Bora C., Dolui S.K., Fabrication of Polypyrrole/Graphene Oxide Nanocomposites by Liquid/Liquid Interfacial Polymerization and Evaluation of Their Optical, Electrical and Electrochemical Properties, *Polymer*, **53**: 923-932 (2012).
- [64] Kuilla T., Bhadra S., Yao D., Kim N.H., Bose S., Lee J.H., Recent Advances in Graphene Based Polymer Composites, *Prog. Polym. Sci.*, **35**: 1350-1375 (2010).
- [65] Lerf A., Klinowski J., Structure of Graphite Oxide Revisited, *J. Phys. Chem. B.*, **102**: 4477- (1998).
- [66] KruegerGrasser R., Weiss A., Selective Liquid Sorption Properties of Hydrophobized Graphite Oxide Nanostructures, *Colloid Polym. Sci.*, **276**: 570-576 (1998).
- [67] Liu P., Xiao M., Preparation and Characterization of Poly(vinyl acetate)-Intercalated Graphite Oxide Nanocomposite, *J. Mater. Chem.*, **10**: 933- (2000).
- [68] Teksoz S., Acar C., Unak P., Hydrolytic Behavior of Th<sup>4+</sup>, UO<sub>2</sub><sup>2+</sup>, and Ce<sup>3+</sup> Ions at Various Temperatures, *J. Chem. Eng. Data*, **54**: 1183-1188 (2009).
- [69] Li Y., Du Q., Liu T., Sun J., Jiao Y., Xia Y., Xia L., Wang Z., Zhang W., Wang K., Zhu H., Wu D., Equilibrium, Kinetic and Thermodynamic Studies on the Adsorption of Phenol onto Graphene, *Materials Research Bulletin*, **47**: 1898-1904 (2012).
- [70] Wang H., Yuan X., Wu Y., Huang H., Zeng G., Liu Y., Wang X., Lin N., Qi Y., Adsorption Characteristics and Behaviors of Graphene Oxide for Zn(II) Removal from Aqueous Solution, *Applied Surface Science*, **279**: 432-440 (2013).
- [71] Liu Y.H., Wang Y.Q., Zhang Z.B., Cao X.H., Nie W.B., Li Q., Hua R., Removal of Uranium from Aqueous Solution by a Low Cost and High-Efficient Adsorbent, *Applied Surface Science*, **273**: 68-74 (2013).
- [72] Anirudhan T.S., Suchithra P.S., Senan P., Tharun A.R., Kinetic Equilibrium Pro-Files of Adsorptive Recovery of Thorium(IV) from Aqueous Solutions Using Poly(methacrylic acid) Grafted Cellulose/Bentonite Superabsorbent Composite, *Industrial & Engineering Chemistry Research*, **51**: 4825- (2012).
- [73] Sheng G., Hu J., Wang X., Sorption Properties of Th(IV) on the Raw Diatomite-Effects of Contact Time, pH, Ionic Strength and Temperature, *Appl. Radiat. Isot.*, **66**: 1313-1320 (2008).

- [74] Moulin C., Amekraz B., Hubert S., Moulin V., Study of Thorium Hydrolysis Species by Electrospray-Ionization Mass Spectrometry, *Analytica Chimica Acta*, **441**: 269-279 (2001).
- [75] Chen C., Wang X., Sorption of Th (IV) to Silica as a Function of pH, Humic/Fulvic Acid, Ionic Strength, Electrolyte Type, *Applied Radiation and Isotopes*, **65**: 155-163 (2007).
- [76] Deng X.J., Lu L.L., Li H.W., Luo F., The Adsorption Properties of Pb(II) and Cd(II) on Functionalized Graphene Prepared by Electrolysis Method, *J. Hazard Mater*, **183**: 923-930 (2010).
- [77] Manos M.J., Kanatzidis M.G., Layered Metal Sulfides Capture Uranium from Seawater, *J. Am. Chem. Soc.*, **134**: 16441-16446 (2012).